Absolute distance measurement in a combined-dispersive interferometer using a femtosecond pulse laser

OPEN ACCESS
IOP Publishing
Measurement Science and Technology
Meas. Sci. Technol. **27** (2016) 015202 (12pp)
doi:10.1088/0957-0233/27/1/015202

Absolute distance measurement in a combined-dispersive interferometer using a femtosecond pulse laser

Hanzhong Wu[1], Fumin Zhang[1], Fei Meng[2], Tingyang Liu[1], Jianshuang Li[2], Liang Pan[3] and Xinghua Qu[1]

[1] State Key Laboratory of Precision Measurement Technology and Instruments, Tianjin University, Tianjin 300072, People's Republic of China
[2] National Institute of Metrology, China, Beijing 100013, People's Republic of China
[3] Key Laboratory of Opto-electronics Information Technology of Ministry of Education, Tianjin University, Tianjin 300072, People's Republic of China

E-mail: zhangfumin@tju.edu.cn

Received 22 July 2015, revised 16 September 2015
Accepted for publication 21 September 2015
Published 24 November 2015

Abstract

In this paper, a ranging system using dispersive interferometry is developed with a femtosecond pulse laser, aiming to eliminate the measurement dead zones by using a greatly unbalanced Mach–Zehnder interferometer. The distance can be measured by the frequency of the spectral modulation. We indicate that the integer number of the pulse-to-pulse length can be determined by changing the repetition frequency. In the short distance measurement, the results show an agreement within 1.5 μm compared with an incremental He-Ne laser in the 1 m measurement range. We do large-scale experiments on a long optical rail using a typical Michelson interferometer, and an agreement well within 25 μm is obtained in a range up to 75 m, corresponding to a relative precision of 3.3×10^{-7}. Additionally, we experimentally optimize the system set-up to minimize the measurement uncertainty.

Keywords: absolute distance measurement, femtosecond pulse laser, dispersive interferometry, uncertainty evaluation

(Some figures may appear in colour only in the online journal)

1. Introduction

The frequency comb has been proven to be very powerful in the field of metrology, such as absolute frequency measurement [1], absolute distance/thickness measurement [2–4], and the refractive index measurement [5], etc. The frequency comb is a pulse light with a stable time interval in the time domain, and comprises a series of discrete and uniform spectral lines in the optical domain, which can be traceable to a time/frequency standard once the repetition frequency and the carrier envelop offset frequency are well locked [6].

In 1983, the speed of light in vacuum was strictly defined as $c = 299{,}792{,}458$ m s^{-1}, and the meter is thus defined as the length light travels in vacuum in $1/c$ s, truly uniting distance ranging and time keeping.

A frequency comb-based ranging system can determine long distances in air, with a high-precision, large non-ambiguity range, and a high up-date rate. During the past decade, researchers have proposed many methods for distance metrology using the frequency comb. First, the distance can be determined by the mode phases, which can be obtained by the inter-mode beat with one single comb laser [7], or multi-heterodyne with dual combs [8]. Second, a technique based on pulse cross correlation can measure distances by Hilbert transform to evaluate the peak position of the fringe packet [9–12], Fourier transform to get the slope of the unwrapped spectral

phase [13], the stationary phase of the chosen wavelength in the spectral range of the comb laser [14–16], the peak shift of the cross-correlation patterns [17, 18], and the interfered intensity [19, 20]. Third, pulse-to-pulse alignment [21–24] can make the pulses in space align with each other precisely, where the unknown distances are strictly the integer multiples of the pulse-to-pulse length. Fourth, dispersive interferometry can determine distances through the derivative of the unwrapped phase of the spectrograms [25–29], which are usually captured by a CCD camera. In addition, a frequency comb can calibrate continuous wave lasers, to improve the accuracy of distance measurement dramatically [30, 31].

We focus on the method of dispersive interferometry, which has already been used in long distance measurement up to 50 m with micrometer precision [27], nanometer resolution [26], and fast responding speed [25]. Despite these advantages, the practical measurement range is actually only tens of millimeters in the vicinity of the multiples of the pulse-to-pulse length due to the limited resolution of the spectrometer, as mentioned in [27], which means previous methods based on only dispersive interferometry can not measure arbitrary distances, leading to a wide dead zone. In addition, there is no discussion about the measurement of the integer number of the pulse-to-pulse length using dispersive interferometry, which can potentially extend the non-ambiguity range of our measurement.

In this paper, a short description of the theory of dispersive interferometry is demonstrated first. After that, we introduce the principles of distance measurement and the measurement of the integer number of pulse-to-pulse length. In the experiments, a combined system is proposed, which is composed of a Michelson interferometer and a highly unbalanced Mach–Zehnder interferometer, which truly enables arbitrary distance measurement only using dispersive interferometry without any dead zones. Our experiment results show an agreement within 1.5 μm in a range of 1 m. The integer number of pulse-to-pulse length can be measured by tuning the repetition frequency of the comb laser. In long distance measurement, an agreement well within 25 μm in a range up to 75 m is achieved, corresponding to a relative precision of 3.3×10^{-7}. Finally, we perform theoretical and experimental optimization of the measurement uncertainty for this widely used method using dispersive interferometry.

2. Measurement principle

2.1. Principle of dispersive interferometry for distance measurement

First, we give a short description of the principle of dispersive interferometry using an unbalanced Michelson interferometer, as shown in figure 1. The pulse train emitted by the comb source is split into two beams, which are recombined after travelling through various optical delays. A spectrometer is used to detect and record the spectrum. The measured distance L is the length difference between the reference beam and the measurement beam.

The comb can be expressed as $E(t)$ in the time domain and $E(\omega)$ in the frequency domain. The center frequency of the frequency comb is ω_c. We record the reference pulse that goes into the reference beam and is reflected by reference mirror M_R as $E_{ref}(t)$, whose spectrum is $E_{ref}(\omega)$ correspondingly. The measurement pulse that goes into the measurement beam and is reflected by target mirror M_T is recorded as $E_{pro}(t)$, and the spectrum is $E_{pro}(\omega)$. The time delay between the reference pulse and the measurement pulse is τ, and the unknown distance L can be thus calculated as $L = c\tau/(2n_g)$. c is the speed of light in vacuum, and n_g is the group refractive index. $n_g = n(\lambda) - \lambda\partial n(\lambda)/\partial\lambda$.

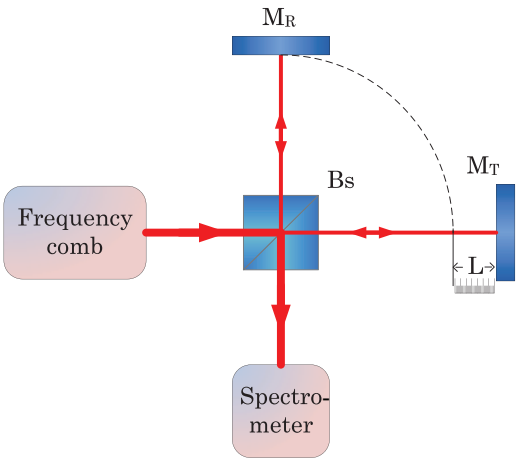

Figure 1. Schematic of the experimental setup.

The spectrum of the reference pulse can be expressed as:

$$E_{ref}(\omega) = \alpha E(\omega). \tag{1}$$

Based on the Fourier transform, the spectrum of the measurement pulse can be expressed as:

$$E_{pro}(\omega) = \beta E(\omega)\exp(-i\tau\omega). \tag{2}$$

Therefore, the power ratio of the reference pulse and the measurement pulse can be expressed as α^2/β^2. Please note that α and β are not constant here, which are spectrally dependent and distance-dependent.

The spectral intensity detected by the spectrometer can be calculated as:

$$\begin{aligned} I(\omega) &= (E_{ref}(\omega) + E_{pro}(\omega))^2 \\ &= \left\langle (E_{ref}(\omega) + E_{pro}(\omega))(E_{ref}(\omega) + E_{pro}(\omega))^* \right\rangle \\ &= |E_{ref}(\omega)|^2 + \left|E_{pro}(\omega)\right|^2 + 2\mathrm{Re}[E_{ref}(\omega)E^*_{pro}(\omega)] \\ &= E^2(\omega)[\alpha^2 + \beta^2 + 2\alpha\beta\cos(\tau\omega)]. \end{aligned} \tag{3}$$

From equation (3), it can be found that the spectral interference fringe consists of two parts: a dc term and an interfered term. The dc intensity of the interference fringe is $(\alpha^2 + \beta^2)E^2(\omega)$, and the interfered term is $2\alpha\beta\cos(\tau\omega)E^2(\omega)$. The values of α and β (i.e. the power ratio of the reference pulse and the measurement pulse) contribute to the modulation depth (contrast) of the spectrograms. The fringes can always reach zero when α equals β, and the modulation depth becomes shallower with increasing the difference between α and β, where a deeper modulation depth is preferred in the data process. From the interfered term, the modulation frequency

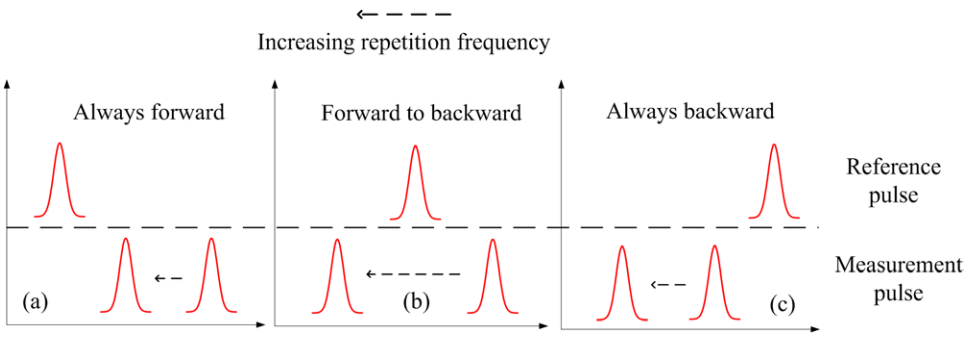

Figure 2. Relative position between the reference pulse and the measurement pulse with increasing repetition frequency. (a) The measurement pulses are always forward; (b) the measurement pulses are shifted backward; (c) the measurement pulses are always backward compared with the reference pulses.

of the interferogram is the time delay τ between the reference pulse and the measurement pulse in fact.

In long-range distance measurement, where L is larger than $L_{pp}/2$ in a Michelson interferometer, the unknown distances can be calculated as:

$$L = \frac{1}{2}\left(N \cdot L_{pp} + \frac{c}{n_g} \cdot \tau\right) \tag{4}$$

where N is the integer number of L_{pp}, and L_{pp} is the pulse-to-pulse length, $L_{pp} = c/(f_{rep}n_g)$, f_{rep} is the repetition frequency of the comb laser, and $n_g = n(\lambda) - \lambda\partial n(\lambda)/\partial\lambda$. According to equation (4), the distance can be determined by precisely measuring N and τ, and τ can be obtained by Fourier transforming the spectrograms.

2.2. Determination of N

In long distance measurement, it is very important to determine the value of the integer number of the pulse-to-pulse length. We can easily determine the value of N by changing the repetition frequency. Here we consider three situations when we tune the repetition frequency slightly, which are shown in figure 2.

Assuming the repetition frequency is increased from f_{rep} to $f_{rep} + \Delta f$, in the case of figure 2(a) the shift displacement of the measurement pulse can be expressed as:

$$d = N \cdot \frac{c}{n_g} \cdot \left(\frac{1}{f_{rep}} - \frac{1}{f_{rep} + \Delta f}\right). \tag{5}$$

According to equation (4), the distance variation we measured by the frequency of the interferogram can be expressed as:

$$d = \frac{c}{n_g} \cdot (\tau_1 - \tau_2) \tag{6}$$

where τ_1 and τ_2 are the time delays between the reference pulse and the measurement pulse before and after increasing the repetition frequency, respectively, which can be obtained through the frequency of the spectral modulation. Uniting equations (5) and (6), N can be calculated as:

$$N = \text{round}\left((\tau_1 - \tau_2) \cdot \frac{f_{rep} \cdot (f_{rep} + \Delta f)}{\Delta f}\right) \tag{7}$$

where *round* indicates the nearest integer.

For the situations in figures 2(b) and (c), N can be precisely calculated similarly to that in figure 2(a). We can thus express N as:

$$N = \begin{cases} \text{round}\left((\tau_1 - \tau_2) \cdot \dfrac{f_{rep} \cdot (f_{rep} + \Delta f)}{\Delta f}\right) & \text{for figure 2(a)} \\ \text{round}\left((\tau_1 + \tau_2) \cdot \dfrac{f_{rep} \cdot (f_{rep} + \Delta f)}{\Delta f}\right) & \text{for figure 2(b)} \\ \text{round}\left((\tau_2 - \tau_1) \cdot \dfrac{f_{rep} \cdot (f_{rep} + \Delta f)}{\Delta f}\right) & \text{for figure 2(c).} \end{cases} \tag{8}$$

It can be found that we do not need to consider the influence of the air refractive index when determining the value of N. We can also measure N by decreasing the repetition frequency of the comb source, according to the derivation shown above. The only difference is that the measurement pulse will go further when the repetition frequency is decreased. We find that, based on the modulation frequency, both the integer and the fractional part of the unknown distances can be determined.

2.3. Principle of distance measurement in an unbalanced Mach–Zehnder interferometer

Due to the limited resolution of the dispersive interferometer, the practical measured length/displacement is only tens of millimeters in the vicinity of the integer multiples of L_{pp}, which is the biggest limitation for the previous schemes based on dispersive interferometry. The key point is to make the time delay between the reference pulse and the measurement pulse small enough in space. We use a greatly unbalanced Mach–Zehnder interferometer to adjust the relative position of the reference pulse and the measurement pulse by tuning the repetition rate of the frequency comb. A sufficiently small time delay between the reference pulse and the measurement pulse can be obtained, which can be reconstructed by a simply dispersive spectrometer. The schematic is shown in figure 3.

In figure 3, the pulse light emitted from the comb source is split into two beams, and one of them travels through an additional delay fiber. We name the beam without the delay fiber Beam A, and that with the delay line Beam B. Beams A and B are combined at the coupler, and finally the interfered fringes

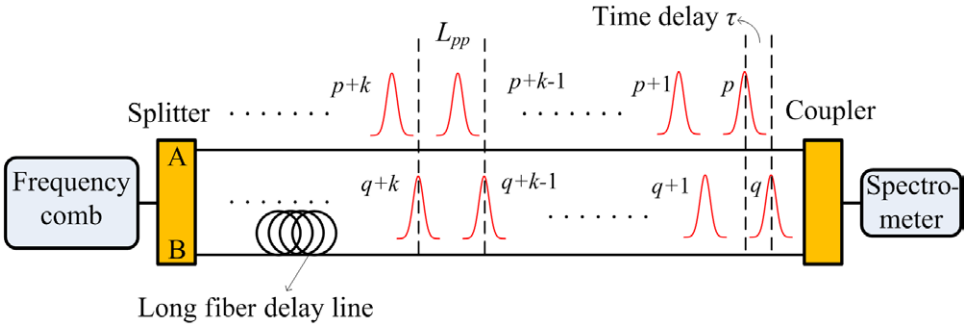

Figure 3. Schematic of tuning the time delay by changing the repetition rate.

are displayed on the spectrometer. We define the index of the closest pulses of Beam A and B as p and q, where we find that the difference m between p and q can be very large, $m = |p–q|$.

When we slightly change the repetition frequency of the frequency comb, i.e. give a small variation to the pulse-to-pulse length, the pulse positions in space will be shifted correspondingly in Beams A and B. Considering the pth pulse in Beam A and the qth pulse in Beam B, when the repetition frequency is changed from f_{rep1} to f_{rep2}, the respective length shift can be expressed as:

$$d_A = \frac{\left|f_{\mathrm{rep1}} - f_{\mathrm{rep2}}\right|}{f_{\mathrm{rep1}} f_{\mathrm{rep2}}} \cdot \frac{c}{n_g} \cdot p \tag{9}$$

$$d_B = \frac{\left|f_{\mathrm{rep1}} - f_{\mathrm{rep2}}\right|}{f_{\mathrm{rep1}} f_{\mathrm{rep2}}} \cdot \frac{c}{n_g} \cdot q. \tag{10}$$

d_A and d_B express the length shift corresponding to the pth pulse in Beam A and the qth pulse in Beam B, respectively. Let us consider the case shown in figure 3, the pulse train in Beam A is delayed to that in Beam B. The temporal interval χ (here χ is the time interval after changing the repetition frequency, and τ is the time delay before changing the repetition rate) between the closest pulses in Beams A and B, i.e. the pth pulse in Beam A and the qth pulse in Beam B, can be calculated as:

$$\chi = \begin{cases} \dfrac{c\tau}{n_g} - (d_B - d_A) = \left(\tau - \dfrac{f_{\mathrm{rep2}} - f_{\mathrm{rep1}}}{f_{\mathrm{rep1}} f_{\mathrm{rep2}}} \cdot m\right) \cdot \dfrac{c}{n_g} & f_{\mathrm{rep2}} > f_{\mathrm{rep1}} \\ \dfrac{c\tau}{n_g} + (d_B - d_A) = \left(\tau + \dfrac{f_{\mathrm{rep1}} - f_{\mathrm{rep2}}}{f_{\mathrm{rep1}} f_{\mathrm{rep2}}} \cdot m\right) \cdot \dfrac{c}{n_g} & f_{\mathrm{rep2}} < f_{\mathrm{rep1}}. \end{cases} \tag{11}$$

τ is the initial time interval. Similar to the above analysis, when Beam A reaches the target later than Beam B before changing the repetition frequency, equation (11) can be recalculated as:

$$\chi = \begin{cases} \dfrac{c\tau}{n_g} + (d_B - d_A) = \left(\tau + \dfrac{f_{\mathrm{rep2}} - f_{\mathrm{rep1}}}{f_{\mathrm{rep1}} f_{\mathrm{rep2}}} \cdot m\right) \cdot \dfrac{c}{n_g} & f_{\mathrm{rep2}} > f_{\mathrm{rep1}} \\ \dfrac{c\tau}{n_g} - (d_B - d_A) = \left(\tau - \dfrac{f_{\mathrm{rep1}} - f_{\mathrm{rep2}}}{f_{\mathrm{rep1}} f_{\mathrm{rep2}}} \cdot m\right) \cdot \dfrac{c}{n_g} & f_{\mathrm{rep2}} < f_{\mathrm{rep1}}. \end{cases} \tag{12}$$

According to equations (11) and (12), *it can be found that* the interval between the pth pulse in Beam A and the qth pulse in Beam B can be changed in a tunable range L_s, which can be calculated as:

$$L_S = \frac{\left|f_{\mathrm{rep1}} - f_{\mathrm{rep2}}\right|}{f_{\mathrm{rep1}} f_{\mathrm{rep2}}} \cdot \frac{c}{n_g} \cdot m. \tag{13}$$

In equation (13), this tunable range is proportional to the repetition frequency variation and the index difference of the closest pulses in Beams A and B, which also implies that a sufficiently small time delay between the pulses can be obtained by changing the repetition frequency for a small amount with a larger m. The tunable range can be easily up to L_{pp}, and arbitrary distances can be measured using equations (4), (8), and (13).

Here we would like to give a theoretical description of the unknown distances based on the simplified schematic shown in figure 4. The comb output is split evenly into two parts. One part emits into an unbalanced Michelson interferometer, which means this beam carries all the distance information. The output of the Michelson interferometer and the other part of the comb source are combined at BS2 before being captured by a spectrometer. Please note that the length difference of the beams in the Michelson interferometer is not the integer multiples of L_{pp} any more. For convenience of explanation, we name the pulse train reflected by the reference mirror and the target corner cube in the Michelson interferometer as PTR and PTT, respectively, and the pulses propagating through the long fiber link as PTS (scanning pulse train). Assuming that when the repetition frequency of the frequency comb is f_{r1}, PTR and PTS fully interfere with each other, and we can obtain a distance of L_{R} by equation (4), which is usually several millimeters. We increase the repetition rate to f_{r2}, to make PTT and PTS overlap in space, and we correspondingly get a result of L_{T}. Please note that PTR, PTT, and PTS can be distinguished by using three shutters in the experiments.

We consider three situations where we make the pulses overlap by changing the repetition frequency, as shown in figure 5. It is immediately clear that the unknown distance can be expressed as:

$$L = \begin{cases} \dfrac{1}{2} \cdot \left[\left(\dfrac{1}{f_{r1}} - \dfrac{1}{f_{r2}}\right) \cdot \dfrac{c \cdot m}{n_g} + (L_{\mathrm{T}} - L_{\mathrm{R}})\right] & \text{for figure 5(a)} \\ \dfrac{1}{2} \cdot \left[\left(\dfrac{1}{f_{r1}} - \dfrac{1}{f_{r2}}\right) \cdot \dfrac{c \cdot m}{n_g} - (L_{\mathrm{T}} + L_{\mathrm{R}})\right] & \text{for figure 5(b)} \\ \dfrac{1}{2} \cdot \left[\left(\dfrac{1}{f_{r1}} - \dfrac{1}{f_{r2}}\right) \cdot \dfrac{c \cdot m}{n_g} - (L_{\mathrm{T}} - L_{\mathrm{R}})\right] & \text{for figure 5(c)}. \end{cases} \tag{14}$$

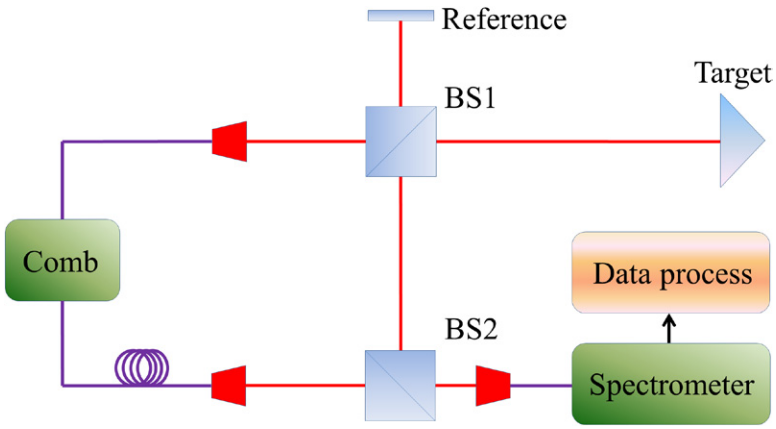

Figure 4. Schematic of the distance measurement system.

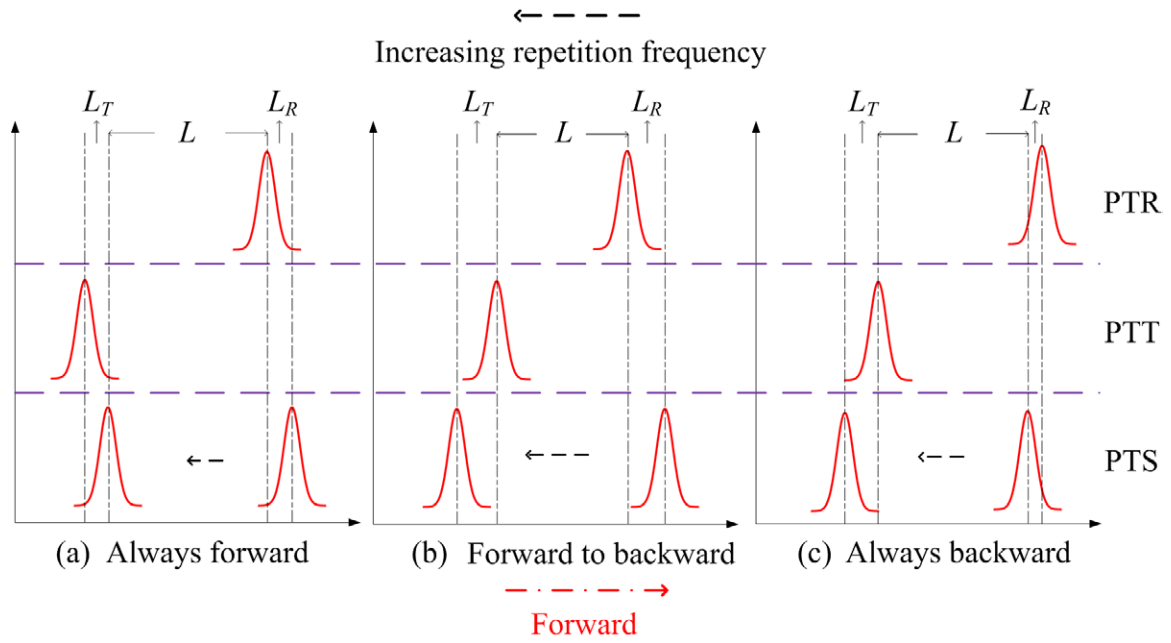

Figure 5. Relative positions between PTR, PTT, and PTS before and after changing the repetition frequency. (a) PTS is always ahead of PTR and PTT; (b) PTS is ahead of PTR, and behind PTT; (c) PTS is always behind PTR and PTT.

3. Experimental setup

Figure 6 shows the experimental setup. We develop a combined ranging system to measure arbitrary distances using a dispersive interferometer. The laser source (for short distance, we use Menlo System FC1500-250-WG; for long distance range, we use Onefive Origami-15) locked to a Rb clock (Stanford FS725) that emits a pulse light into the interferometer from Ports A and B. The beam of Port A is collimated into a Michelson interferometer. The beam of Port B externally propagates through a 2 km extra fiber delay line (1.8 km simple fiber and 0.2 km dispersion compensating fiber DCF), where careful design should be performed to suppress the fiber noise. We use a compact vibration isolation platform (minus-k 25BM-10) and a hermetically sealed enclosure with dual stage temperature stabilization to eliminate the vibration and the thermal change in the environment. The output of the Michelson interferometer and the beam of Port B are combined at BS2. S1, S2, and S3 are three shutters, which can change the working mode of the system. A frequency counter (Agilent 53220A) is applied to measure the repetition frequency of the frequency comb, and a dispersive spectrometer (YOKOGAWA AQ6370D-20) is used to detect and record the spectral interferograms. The interfered fringe packets are Fourier transformed to obtain the spectrogram frequency, and to determine the distances. We use a cw counting interferometer (Agilent 5519B) to verify the distance measurement results. The target corner cubes of our dispersive interferometer and the He-Ne laser are fixed on a small PC-controlled carriage. Both the measurement beams of the dispersive interferometer and the cw counting distance meter are aligned to be strictly parallel to the long rail. Since the distance meter can only measure distances incrementally, we first reset the cw counting interferometer at the initial position (reference zero position of He-Ne), giving the absolute distance of L_0 for the dispersive interferometer, and then move the target mirror to the next position of the distance of L, providing changing length

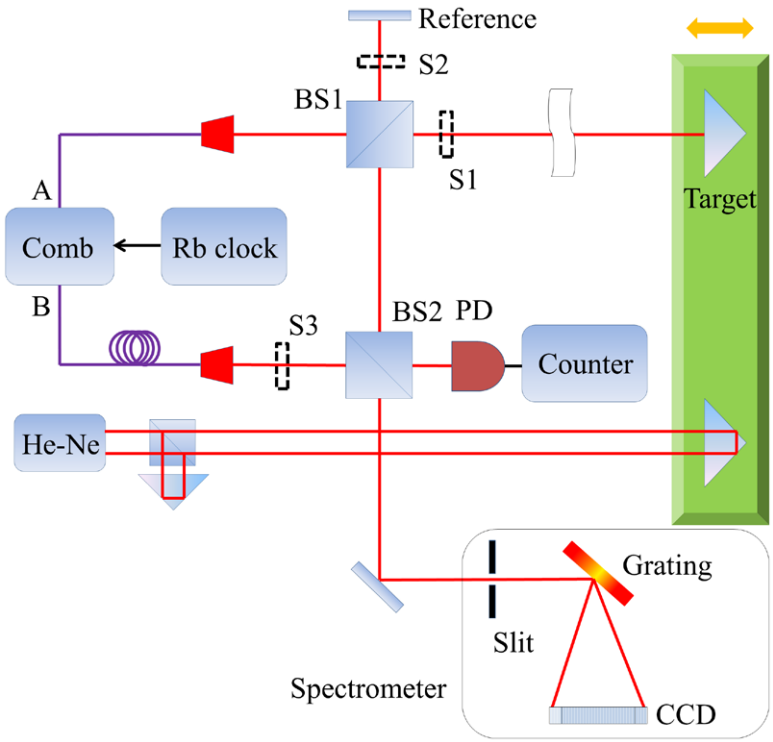

Figure 6. Experimental setup.

$\Delta L = L–L_0$. Then we can compare the measurement results of He-Ne and our dispersive interferometer.

4. Experimental results

4.1. Short distance measurement

We carry out short distance measurement only up to 1 m due to the limited space in our lab. Our objective is to show that this system can measure arbitrary distances. Figure 7 denotes the spectrum of the laser source with a center wavelength of about 1560 nm and a spectral width of about 50 nm. The environment conditions are 24.1 °C, 1001.4hPa, and 72.3% humidity. The group refractive index of air can be calculated to be 1.000 2622 based on the Ciddor formula [32].

We estimate the value of m. In our experiments, before combined at BS2, the light beam reflected by the reference mirror in the Michelson interferometer has passed through about 3 m optical path in air, and the pulse train travelling through the 2 km fiber link takes a total optical path length of about 2939.7 m. m can be thus estimated to be:

$$m = \text{round}\left(\frac{2939.7 - 3}{L_{\text{pp}}}\right) = 2447. \tag{15}$$

In equation (15), L_{pp} is approximately 1.2 m. In our experiments, we first close S1, open S2 and S3, and increase the repetition frequency with 200 Hz step size to observe the spectrograms, where it is easy to judge the relative position between the pulses. When the spectrogram can be observed on the spectrometer, we can find that the spectrogram frequency decreases first and then increases again with increasing repetition frequency until the modulation disappears. Based on the analysis in section 2.1, the spectrogram frequency is proportional to the time interval of the pulses. We can thus say, when we increase the repetition frequency, a rising spectrogram frequency denotes that PTS is behind PTR, while a dropping frequency indicates that PTS is ahead of PTR. In our experiments, we carefully tune the repetition frequency to make sure that PTS is always ahead of PTR and PTT, which means we should use the first case in equation (14) to determine the distances.

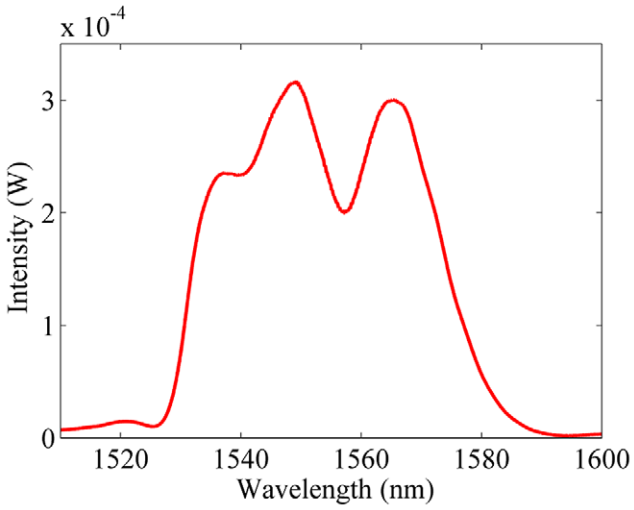

Figure 7. Spectrum of the pulse source.

After recording the current repetition frequency and the spectrograms, S2 is closed, and S1 and S3 are open. The measurement beam is initially set to be a little longer

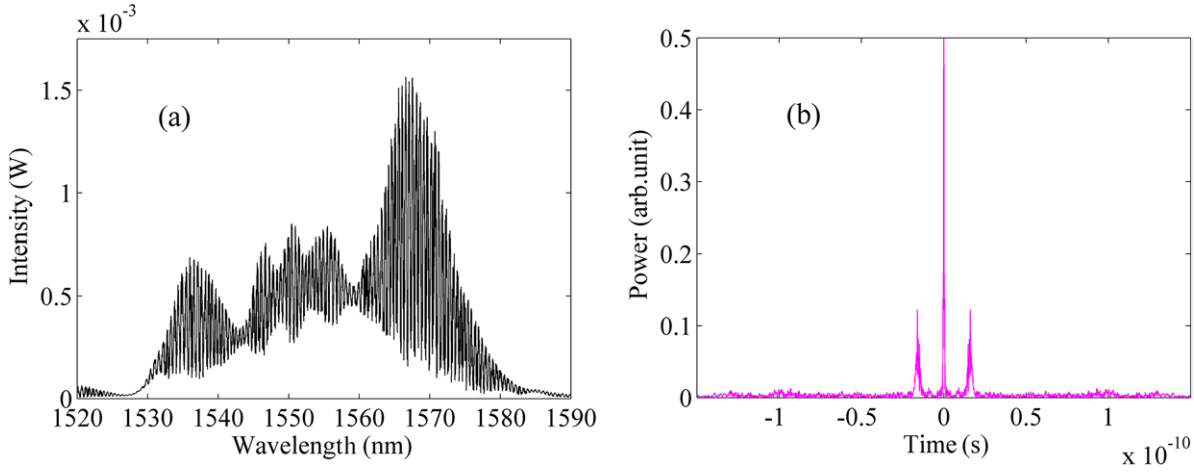

Figure 8. Spectrogram generated by PTR and PTS, and the result of the Fourier transform. The current repetition frequency is 250.057 899 MHz, and the spectrogram frequency is 1.606×10^{-11} Hz.

than the reference beam in the Michelson interferometer in our case. Hence, we increase the repetition frequency until the interference fringes can be observed again. We correspondingly record the current repetition frequency and the spectrograms. The spectrograms are processed to get the modulation frequency, and finally the distance can be measured using equation (14). Figure 8 shows the spectrogram generated by PTR and PTS, and the result of Fourier transform. Figure 9 shows the spectrogram generated by PTT and PTS at the position of the equal arm, and the corresponding result of the Fourier transform. According to equation (4), the initial distance can be calculated to be 1.423 mm.

We move the target corner cube by about 0.1 m, increase the repetition frequency, and observe the spectrogram. The spectral modulation and the result of the Fourier transform are shown in figure 10. The distance can be calculated to be 98.462 mm using equations (4) and (14), indicating a length increment of 97.038 mm. Finally an agreement of 0.304 μm is achieved, compared with a reference cw counting interferometer.

Due to the limited space in our lab, we move the stage 9 times with a step size of about 0.1 m. At each position, we quickly measure the distance 5 times, and record the current repetition frequency and the spectrograms. One single measurement needs 2 s measuring time. The comparison between our dispersive ranging system and the reference incremental interferometer is shown in figure 11, where the midpoints are the average of 5 measurements, and the errorbars denote the standard deviation with a 2 s measuring time. We find that an agreement within 1.5 μm is achieved, corresponding to a relative precision of 1.6×10^{-6}.

4.2. Measurement of N

As a proof of principle, we carry out experiments corresponding to the three situations, as shown in figure 2, respectively. In this section, we close S3, and open S1 and S2, which means the Michelson interferometer can work well. The target is moved to the location where the arm length difference of the Michelson interferometer is about 1.2 m, i.e. N equals to 2. Table 1 shows the experimental results.

According to equation (8), for all three situations, N can be uniquely determined as:

$$\begin{aligned} N_{(a)} &= \text{round}\left[(1.267 \times 10^{-11} - 0.5792 \times 10^{-11}) \right. \\ &\quad \left. \times \frac{249.380133 \times 249.5932475 \times 10^6}{249.5932475 - 249.380133}\right] \\ &= \text{round}(2.0088) = 2 \end{aligned} \tag{16}$$

$$\begin{aligned} N_{(b)} &= \text{round}\left[(1.099 \times 10^{-11} + 0.5792 \times 10^{-11}) \right. \\ &\quad \left. \times \frac{250.116956 \times 249.5932475 \times 10^6}{250.116956 - 249.5932475}\right] \\ &= \text{round}(2.0005) = 2 \end{aligned} \tag{17}$$

$$\begin{aligned} N_{(c)} &= \text{round}\left[(2.431 \times 10^{-11} - 2.107 \times 10^{-11}) \right. \\ &\quad \left. \times \frac{250.116956 \times 250.016956 \times 10^6}{250.116956 - 250.016956}\right] \\ &= \text{round}(2.0261) = 2. \end{aligned} \tag{18}$$

We find that the integer number of L_{pp} can be determined precisely using our method.

4.3. Long distance measurement

We carry out long distance measurement on the long optical tunnel underground in the National Institute of Metrology. We use a compact femtosecond pulse laser (Onefive Origami-15) in this case, out of our lab. The environmental conditions are well controlled, which are 24.4 °C, 1007.6hPa, and 41.9% humidity. The stability of the He-Ne interferometer is below 0.2 μm for 10 s, and below 0.8 μm for 10 min with a distance of 80 m, and below 70 nm at 2 m distance. Figure 12 shows the practical experimental photograph.

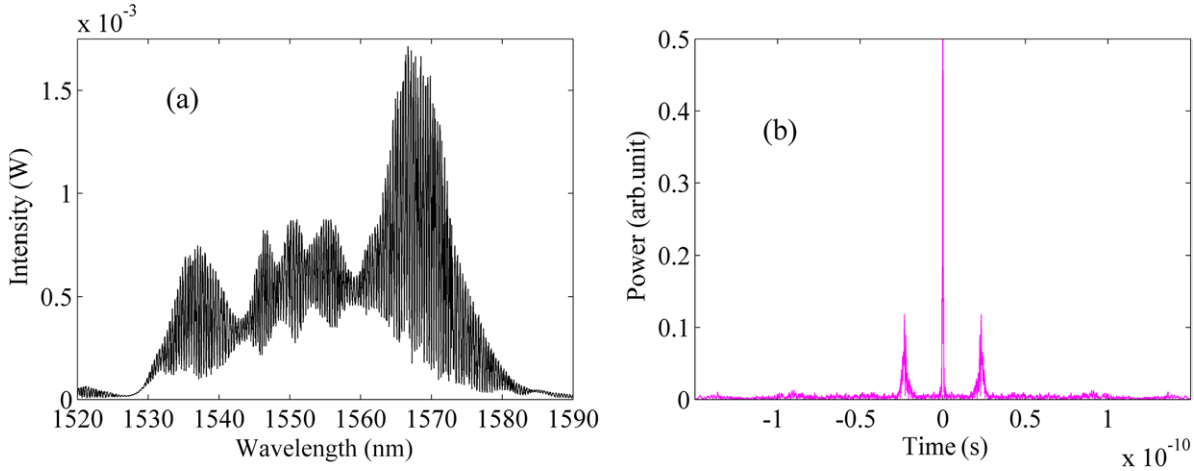

Figure 9. Spectrogram generated by PTT and PTS, and the result of the Fourier transform. The current repetition frequency is 250.057 899 MHz, and the spectrogram frequency is 2.556×10^{-11} Hz.

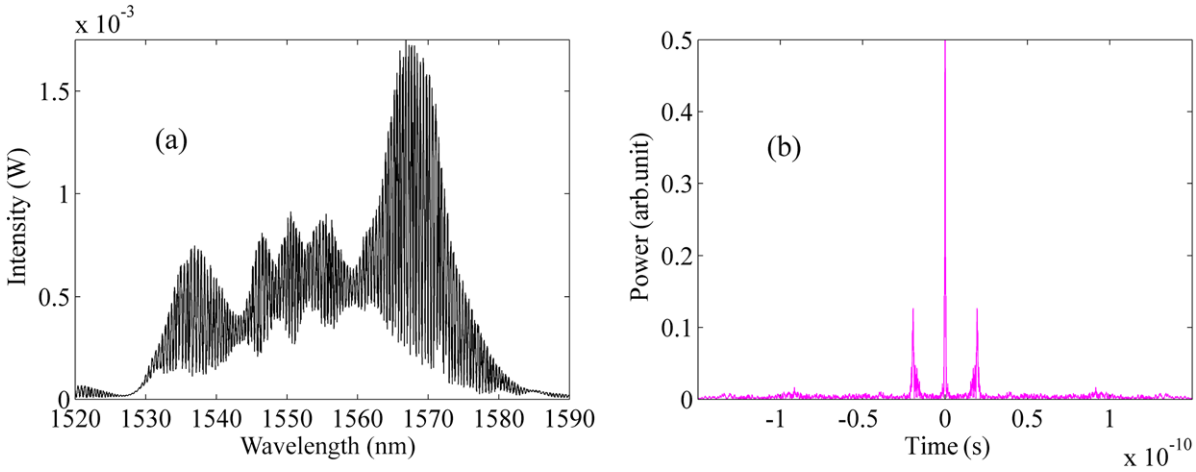

Figure 10. Spectrogram generated by PTT and PTS in the distance of about 0.1 m, and the result of the Fourier transform. The current repetition frequency is 250.074 604 MHz, and the spectrogram frequency is 1.941×10^{-11} Hz.

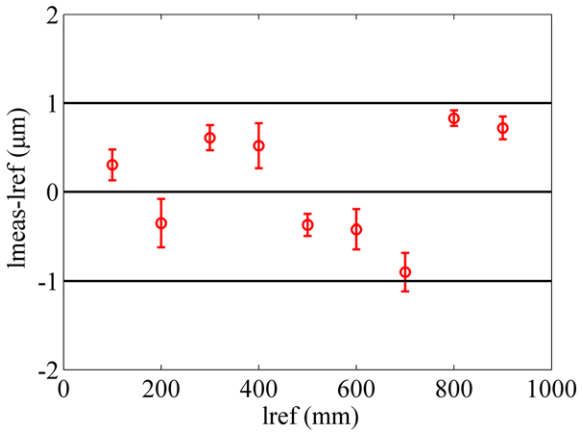

Figure 11. Ranging results compared with a cw counting interferometer.

Figure 13 shows the spectrum of the light source we use in the long distance case, with the center wavelength of 1560 nm and the bandwidth of about 55 nm. The group refractive index of air is correspondingly calculated to be 1.000 26388 based on the Ciddor formula.

We use equation (4) to determine the distances. The measurement process is described simply in section 3. Figure 14 shows the spectrograms corresponding to positions of 1.8 m and 75 m, respectively, which are Fourier transformed to pick the frequencies to measure distances.

From figure 14 we find that the total intensity of the spectrum and the spectral modulation depth drop dramatically after a distance of 75 m (150 m optical path). We move the small car first by 3 m step size with distances less than about 28 m, and then by 6 m step size until the end of the tunnel. Each distance is quickly measured 5 times, within a 15 s measuring time for one single measurement, and using a fixed setup of the spectrometer. The scatters are plotted in figure 15.

The comparison between our ranging system and the reference incremental interferometer is shown in figure 16, where the midpoints are the average of five single measurements, and the errorbars indicate the standard deviations with an averaging time of 15 s. We find that in a range up to 75 m, an agreement well within 25 μm is reached, corresponding to a relative precision of 3.3×10^{-7}, which is a better result below 10^{-6}.

Table 1. Experimental results to determine the value of N.

(a) Always forward			
Repetition frequency (MHz)		Spectrogram frequency (10^{-11} Hz)	
Before changing	After changing	Before changing	After changing
249.380 133	249.593 2475	1.267	0.5792
(b) Forward to backward			
Repetition frequency (MHz)		Spectrogram frequency (10^{-11} Hz)	
Before changing	After changing	Before changing	After changing
249.593 2475	250.116 956	0.5792	1.099
(c) Always backward			
Repetition frequency (MHz)		Spectrogram frequency (10^{-11} Hz)	
Before changing	After changing	Before changing	After changing
250.016 956	250.116 956	2.107	2.431

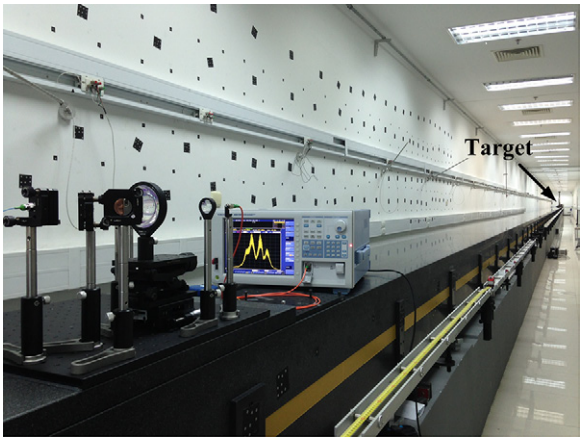

Figure 12. Experimental photograph.

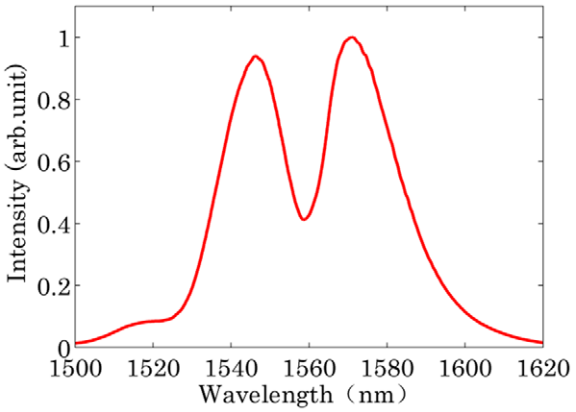

Figure 13. Spectrum of the Onefive Origami-15 pulse laser.

5. Uncertainty evaluation

In this section, we evaluate the measurement uncertainty in detail, and experimentally optimize the system setup, aiming to minimize the uncertainty. Our analysis starts from equation (4). Equation (4) can be rewritten as:

$$L = \frac{1}{2} \cdot \frac{c}{n_g} \cdot \left(\frac{N}{f_{\text{rep}}} + \tau \right). \tag{19}$$

τ is the modulation frequency of the spectral interferograms. Based on the experiments in section 4.2, we get that N can be determined precisely with uncertainty below 1. According to equation (19), the measurement uncertainty of L can be calculated as:

$$u_L = \sqrt{\left(\frac{L}{n_g} u_{n_g} \right)^2 + \left(\frac{c \cdot N}{2n_g \cdot {f_{\text{rep}}}^2} u_{f_{\text{rep}}} \right)^2 + \left(\frac{c}{2n_g} u_\tau \right)^2}. \tag{20}$$

Based on equation (20), we find that the measurement uncertainty of L is mainly related to the refractive index of air, the repetition frequency of the laser source, and the modulation frequency of the spectrograms.

The individual contributions of the various sources are summarized in table 2. We find that the uncertainty related to the modulation frequency contributes dominantly to the combined uncertainty, which is observed to be 24.1 μm constantly based on our experimental results corresponding to 1.6×10^{-13} Hz uncertainty of the modulation frequency of the spectrograms. The uncertainty of the Rb clock is 2×10^{-11}. Due to the phase-locking frequency transfer and possible frequency instability, it is reasonable to assume an uncertainty of 10^{-10}. The uncertainty related to the repetition frequency can be thus expressed as $10^{-10} \cdot L$, which can be neglected. The uncertainty related to the air refractive index is distance dependent. In our experiments, the refractive index of air for both the reference distance meter and the dispersive interferometer is corrected by the Ciddor formula based on the same environment sensors. The contribution of the air refractive index is finally found to be $6.7 \times 10^{-8} \cdot L$ with the well-measured parameters of temperature, pressure, and humidity. Since the experimental results are shown using the comparison between the dispersive interferometer and the cw counting interferometer, it is necessary to measure the uncertainty related to the long optical rail itself, which is found to be below 0.8 μm in the 80 m range. Overall, the combined uncertainty with a coverage factor of $k = 1$ can be represented as $\sqrt{(24.1\mu m)^2 + (6.7 \times 10^{-8} \cdot L)^2}$, corresponding to a relative precision of 3.3×10^{-7} in a range of 75 m.

The third term in equation (20) is related to the uncertainty of the modulation frequency, measured by a simply dispersive

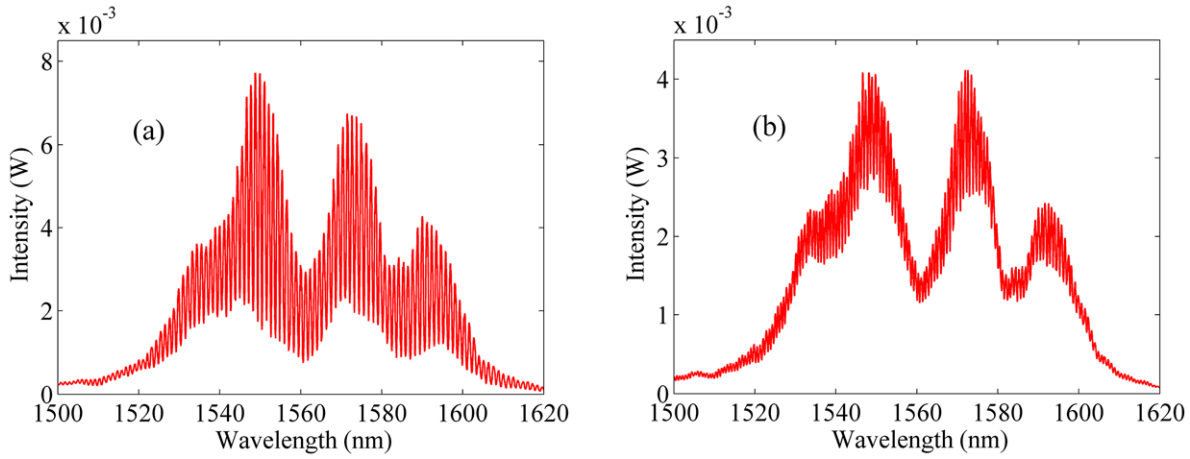

Figure 14. Spectrograms measured on the long rail. (a) 1.8 m location; (b) 75 m location.

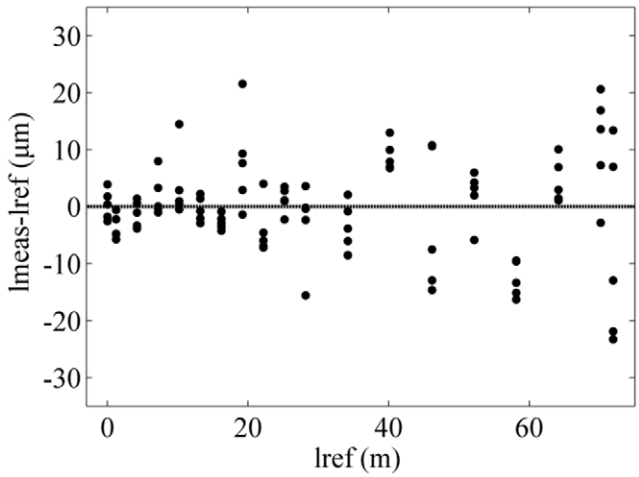

Figure 15. Experimental results in a range up to 75 m.

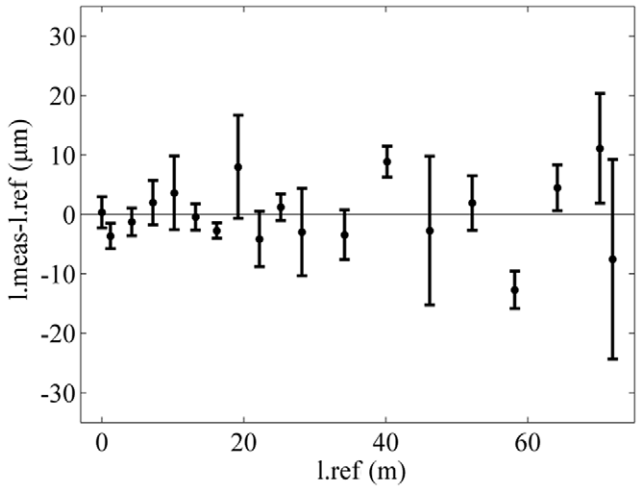

Figure 16. Experimental results compared with a cw counting distance meter.

spectrometer. Generally, the air turbulence, the random vibration of the optical rail, and the environment mutations can all contribute to this term, and can hardly be ultra-perfectly controlled. This is also the reason to achieve extremely high accuracy (relative precision of below 10^{-6}) in a large range (up to tens of meters) is very difficult, even in the laboratory environment. Additionally, we are concerned that the width of the slit in the spectrometer, the scanning speed, the data integration time, and the beam intensity can all affect the uncertainty of the measured spectrogram frequency, further to the uncertainty of the distance measurement.

Table 2. Uncertainty evaluation of the absolute distance measurement.

Sources of the measurement uncertainty	Value
Uncertainty related to the modulation frequency	24.1 μm
Uncertainty of the modulation frequency	1.6×10^{-13} Hz
Uncertainty related to the repetition frequency	$10^{-10} \cdot L$
Uncertainty of the repetition frequency	2×10^{-11}
Uncertainty related to the air refractive index	$6.7 \times 10^{-8} \cdot L$
Uncertainty of temperature	0.07 K
Uncertainty of pressure	6.5 Pa
Uncertainty of humidity	0.3%
Uncertainty related to the long optical rail	0.8 μm
Combined uncertainty ($k = 1$)	$\sqrt{(24.1\mu\text{m})^2 + (6.7 \times 10^{-8} \cdot L)^2}$

We carry out experiments at a position of about 1.2 m in our lab. First we examine the contribution of the slit width to the uncertainty. The scanning speed and the integration time of the curve are set to be 15 s/100 nm, and 15 s/5000 samples. Figure 17 shows the experimental results with 5 single measurements corresponding to different slit widths of the spectrometer, where we find that the standard deviations can be below 1 μm when the slit width is narrower than 0.2 μm.

Figure 18 indicates the results with five measurements when we continuously change the scanning speed of the spectrometer. The slit width is fixed to be 0.02 μm,

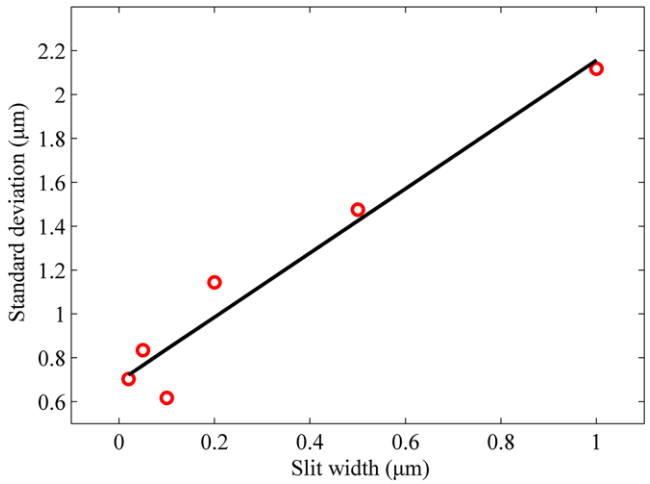

Figure 17. Standard deviation versus slit width.

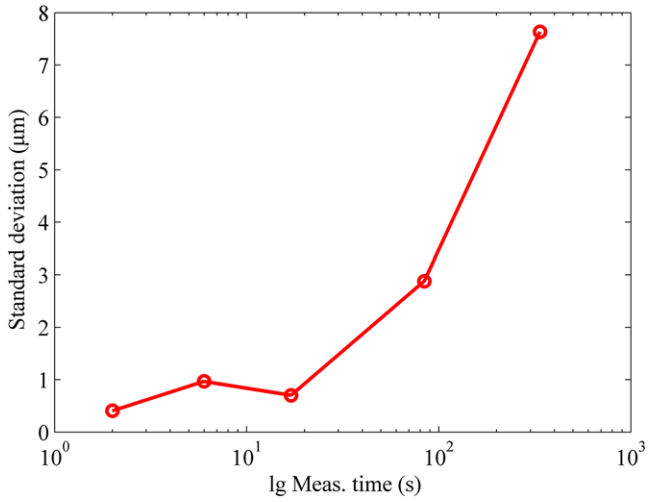

Figure 18. Standard deviation versus scanning speed.

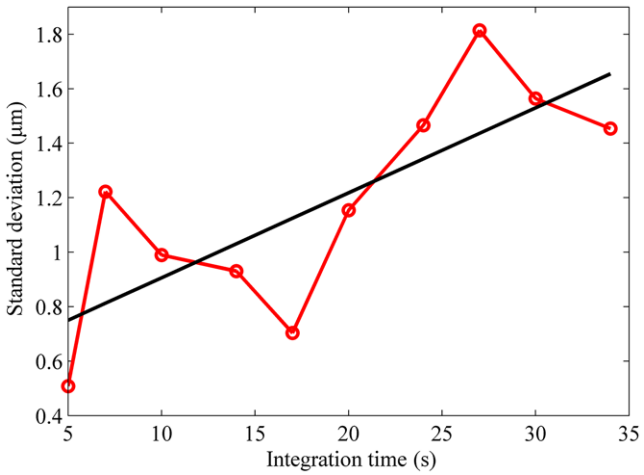

Figure 19. Standard deviation versus integration time.

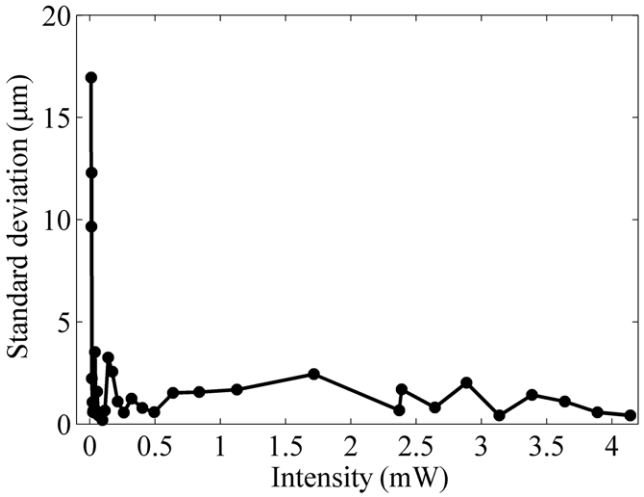

Figure 20. Standard deviation versus beam intensity.

and the integration time of the spectral curve is set to be 15 s/5000 samples. It is clear that the standard deviation can be well below 1 μm when the scanning speed is faster than 15 s/100 nm.

With a 0.02 μm slit width and a 15 s/100 nm scanning speed, we change the integration samples from 1000 to 10 000, corresponding to the integration time from 5 s to 35 s. It can be found that the standard deviation is better when the integration time is less than 15 s, indicating that fast measurement is needed in high accuracy metrology.

We change the beam intensity consecutively by using a neutral filter, from 4.14 mW to 10.6 μW. In figure 20, it is shown that higher intensity will lead to a better standard deviation. We find that the standard deviation is well below 1 μm when the beam intensity is above 3.5 mW. The standard deviation rises drastically to 17 μm when the intensity is less than 50 μW in our case, due to the poor signal-to-noise ratio of the spectral interferograms.

Overall, a 0.02 μm slit width, $a < 15$ s/100 nm scanning speed, $a < 15$ s integration time, and a higher beam intensity are recommended when we use a simply dispersive spectrometer in the case of distance metrology. Please note that the system configurations mentioned above could be different when using a different spectrometer to measure the spectrograms.

6. Conclusion

We develop a combined dispersive ranging system, in which we use a greatly unbalanced Mach–Zehnder interferometer to make the relative time delay between the measurement pulse and the reference pulse sufficiently small by changing the repetition frequency of the comb source, truly enabling arbitrary distance measurement using only dispersive interferometry. We indicate that in long distance measurement the integer number of the pulse-to-pulse length can be measured with an uncertainty below 1. As a proof of principle, we carry out short distance measurement with a 0.1 m interval in our lab, and the experimental results show an agreement within 1.5 μm with a distance of about 1 m, compared with a reference cw counting distance meter. We examine the ability of our method in long distance measurement on an optical rail. The ranging results indicate an agreement well within 25 μm in a range up to 75 m, corresponding to a relative precision

of 3.3×10^{-7}. To minimize the measurement uncertainty, we experimentally evaluate the standard deviations corresponding to difference setups of the dispersive spectrometer and different beam intensities. Our experimental results denote that a 0.02 μm slit width, a $<$ 15 s/100 nm scanning speed, $a < 15$ s integration time, and a higher beam intensity are preferred in our case of distance metrology.

Acknowledgments

We would like to thank Mr Petr Balling in the Czech Metrology Institute for his guidance. We thank the Division of Length and Precision Engineering, the National Institute of Metrology for the support of the long optical tunnel. This work is supported by the National Natural Science Foundation of China (Grant No. 51327006 and 51105274), the Tianjin Research Program of Application Foundation and Advanced Technology (No. 15JCZDJC39300), and the Tianjin Program for Strengthening Marine Technology (KJXH201308).

References

[1] Udem T, Holzwarth R and Hansch T W 2002 Optical frequency metrology *Nature* **416** 233–7
[2] Newbury N R 2011 Searching for applications with a fine-tooth comb *Nat. Photon.* **5** 186–8
[3] Jin J, Kim J W, Kang C, Kim J and Eom T B 2010 Thickness and refractive index measurement of silicon wafer based on an optical comb *Opt. Express* **18** 18339–46
[4] Maeng S, Park J, Jin B O and Jin J 2013 Uncertainty improvement of geometrical thickness and refractive index measurement of a silicon wafer using a femtosecond pulse laser *Opt. Express* **20** 12184–90
[5] Wu G, Takahashi M, Arai K, Inaba H and Minoshima K 2013 Extremely high-accuracy correction of air refractive index using two-color optical frequency combs *Sci. Rep.* **3** 1894
[6] Cundiff S T and Ye J 2003 Colloquium: Femtosecond optical frequency combs *Rev. Mod. Phys.* **75** 325–42
[7] Minoshima K and Matsumoto H 2000 High-accuracy measurement of 240-m distance in an optical tunnel by use of a compact femtosecond laser *Appl. Opt.* **39** 5512–17
[8] Yang R, Pollinger F, Meiners-Hagen K, Tan J and Bosse H 2014 Heterodyne multi-wavelength absolute interferometry based on a cavity-enhanced electro-optic frequency comb pair *Opt. Lett.* **39** 5834–37
[9] Cui M, Zeitouny M G, Bhattacharya N, van den Berg S A, Urbach H P and Braat J J M 2009 High-accuracy long-distance measurements in air with a frequency comb laser *Opt. Lett.* **34** 1982–84
[10] Wei D, Takahashi S, Takamasu K and Matsumoto H 2011 Time-of-flight method using multiple pulse train interference as a time recorder *Opt. Express* **19** 4881–89
[11] Coddington I, Swann W C, Nenadovic L and Newbury N R 2009 Rapid and precise absolute distance measurements at long range *Nat. Photon.* **3** 351–6
[12] Wei D, Takahashi S, Takamasu K and Matsumoto H 2009 Analysis of the temporal coherence function of a femtosecond optical frequency comb *Opt. Express* **17** 7011–18
[13] Lee J, Han S, Lee K, Bae E, Kim S, Lee S, Kim S and Kim Y 2013 Absolute distance measurement by dual-comb interferometry with adjustable synthetic wavelength *Meas. Sci. Technol.* **24** 045201
[14] Zeitouny M G, Cui M, Bhattacharya N, Urbach H P, van den Berg S A and Janssen A J E M 2010 From a discrete to a continuous model for inter pulse interference with a frequency-comb laser *Phys. Rev.* A **82** 023808
[15] Balling P, Mašika P, Křen P and Doležal M 2012 Length and refractive index measurement by Fourier transform interferometry and frequency comb spectroscopy *Meas. Sci. Technol.* **23** 094001
[16] Balling P, Křen P, Mašika P and van den Berg S A 2009 Femtosecond frequency comb based distance measurement in air *Opt. Express* **17** 9300–13
[17] Matsumoto H, Wang X, Takamasu K, and Aoto T 2012 Absolute measurement of baselines up to 403 m using heterodyne temporal coherence interferometer with optical frequency comb *Appl. Phys. Express* **5** 046601
[18] Wang X, Takahashi S, Takamasu K and Matsumoto H 2012 Space position measurement using long-path heterodyne interferometer with optical frequency comb *Opt. Express* **20** 2725–32
[19] Wu H, Zhang F, Cao S, Xing S and Qu X 2014 Absolute distance measurement by intensity detection using a mode-locked femtosecond pulse laser *Opt. Express* **22** 10380–97
[20] Wu H, Zhang F, Li J, Cao S, Meng X and Qu X 2015 Intensity evaluation using a femtosecond pulse laser for absolute distance measurement *Appl. Opt.* **54** 5581–90
[21] Wu G, Takahashi M, Inaba H and Minoshima K 2013 Pulse-to-pulse alignment technique based on synthetic-wavelength interferometry of optical frequency combs for distance measurement *Opt. Lett.* **38** 2140–43
[22] Lee J, Kim Y J, Lee K, Lee S and Kim S W 2010 Time-of-flight measurement with femtosecond light pulses *Nat. Photon.* **4** 716–20
[23] Ye J 2004 Absolute measurement of a long, arbitrary distance to less than an optical fringe *Opt. Lett.* **29** 1153–55
[24] Zhu J, Cui P, Guo Y, Yang L and Lin J 2015 Pulse-to-pulse alignment based on interference fringes and the second-order temporal coherence function of optical frequency combs for distance measurement *Opt. Express* **23** 13069–81
[25] van den Berg S A, Persijn S T, Kok G J P, Zeitouny M G and Bhattacharya N 2012 Many-wavelength interferometry with thousands of lasers for absolute distance measurement *Phys. Rev. Lett.* **108** 183901
[26] Joo K and Kim S 2006 Absolute distance measurement by dispersive interferometry using a femtosecond pulse laser *Opt. Express* **14** 5954–60
[27] Cui M, Zeitouny M G, Bhattacharya N, van den Berg S A and Urbach H P 2011 Long distance measurement with femtosecond pulse using a dispersive interferometer *Opt. Express* **19** 6549–62
[28] Wu H, Cao S, Zhang F and Qu X 2015 Spectral interferometry based absolute distance measurement using frequency comb *Acta Phys. Sin.* **64** 020601
[29] Joo K, Kim Y and Kim S 2008 Distance measurement by combined method based on a femtosecond pulse laser *Opt. Express* **16** 19799–806
[30] Salvadé Y, Schuhler N, Lévêque S and Floch S L 2008 High-accuracy absolute distance measurement using frequency comb referenced multiwavelength source *Appl Opt.* **47** 2715–20
[31] Schuhler N, Salvadé Y, Lévêque S, Dändliker R and Holzwarth R 2006 Frequency-comb-referenced two-wavelength source for absolute distance measurement *Opt. Lett.* **31** 3101–3
[32] Ciddor P E 1996 Refractive index of air: new equations for the visible and near infrared *Appl. Opt.* **35** 1566–73